Generation of ultrashort x-ray pulses

D. G. Stearns, O. L. Landen, E. M. Campbell, and J. H. Scofield
Lawrence Livermore National Laboratory, P.O. Box 808, Livermore, California 94550
(Received 27 July 1987)

We report on the characterization of ultrashort (<10 psec at 1 keV), high-brightness (10^{20} photons/sec mm^2 eV into 2π sr at 1 keV) x-ray pulses. The pulses are generated by exciting a preformed laser-produced plasma using an ~ 1 GW, picosecond laser pulse. Time-resolved measurements of the x-ray emission from a solid Au target are presented as well as the variation in the yield with laser energy and the angle of incidence. Time-integrated x-ray emission yields and spectra are presented for Si, Ti, and Au solid targets. Physical mechanisms responsible for the x-ray generation are discussed.

INTRODUCTION

The development of short pulse lasers ($\tau \leq 1$ psec) has spurred great interest in applying pulse-probe techniques to measure time-resolved phenomena with picosecond, and in some cases subpicosecond, resolution.[1] These experiments generally investigate the interaction of a system with the laser radiation, typically in the visible spectrum. A new important class of time-resolved measurements in plasma and solid-state physics will become possible using ultrashort pulses at x-ray wavelengths.[2–4] The availability of picosecond x-ray pulses will have significant impact in areas such as time-resolved x-ray diffraction and extended x-ray-absorption fine structure (EXAFS), and will provide an ideal source for calibrating time-resolved x-ray detectors such as streak cameras and framing cameras. In this paper we report on the generation of ultrashort x-ray pulses by first heating a solid target with a low-intensity nanosecond laser pulse to produce a low-temperature plasma, followed by excitation of the plasma using a high-power picosecond laser pulse.

EXPERIMENT

The experimental configuration used to generate and characterize the short-pulse x-ray emission is shown in Fig. 1. A short optical pulse of ~ 1 mJ energy in 1 psec at a wavelength of 0.585 μm was provided by an amplified synchronously-pumped mode-locked dye laser, operated at a repetition rate of 2.5 Hz. The amplified pulse width was measured using an autocorrelator. In the majority of the experiments, the short pulse was preceded 3 nsec in time by a long pulse of 3-nsec full width of half maximum (FWHM) duration, containing ~ 15 μJ of energy, generated from the amplified spontaneous emission of the dye amplifier. The long pulse was monitored using a GaAs photoconductive detector (~ 300-psec resolution) with a Tektronix 7104 oscilloscope. The total laser energy was measured on each shot with a calibrated diode.

The laser beam was focused with a f/7.5 lens onto a solid target such that 80% of the laser energy was in a 25-μm-diam spot, determined from the energy transmitted through a pinhole. This produced typical laser intensities of 10^{14} and 10^9 W/cm^2 for the short and long pulses, respectively. The targets consisted of a thin film (>500 Å) of Ti or Au deposited on a polished silicon wafer. An uncoated wafer served as a Si target. The target was mounted on remotely-driven x-y stages and was continuously rastered so that each laser shot was incident on a fresh region of the surface.

The time-integrated x-ray emission spectra were obtained using a 2000-Å–period gold transmission grating as a dispersive element.[5] The grating was positioned normal to the incident radiation, 5 cm from the target. The radiation dispersed into first order was scanned with a channeltron detector positioned 25 cm from the target and mounted on a remotely-driven stage. The channel-

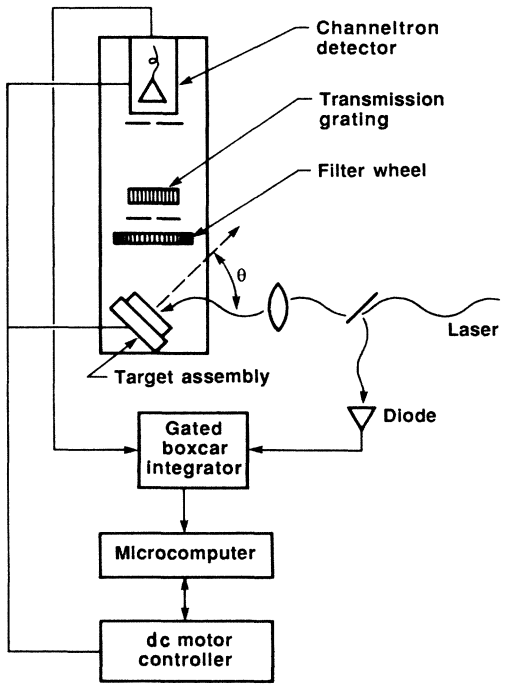

FIG. 1. The configuration of the experiment.

tron was a Galileo model CEM 4730 operated in the analog output mode. Slits of 20 and 100 μm width were placed directly in front of the grating and channeltron, respectively. The slits combined with the source size defined the spectral resolution. It has been previously observed[6] that the emitting region for x-ray energies greater than 250 eV was less than 25 μm in diameter. We assume that the emitting region for softer x rays was no greater in extent than the damage spot on the target of typically ~ 100 μm diameter. Then the spectral resolution $E/\Delta E$ ($\lambda/\Delta\lambda$) for the system was 80 at 40 eV (300 Å), decreasing to 14 at 800 eV (15 Å). Broadband energy discrimination was provided by a filter wheel positioned between the target and the grating. The target assembly, grating, and channeltron detector were mounted on a support bracket that was free to rotate about the laser focus position. This made it possible to easily vary the angle of incidence of the laser beam on the target. In addition, the target assembly could be independently rotated in order to vary the angle of the line of sight of the channeltron detector. The entire assembly was housed in a vacuum chamber routinely pumped to a base pressure of 10^{-5} torr.

The focus of the laser beam on the target was adjusted prior to each scan. The "best focus" was determined by maximizing the x-ray yield as measured in the zeroth order of the transmission grating. A spectrum was collected by slowly scanning the channeltron through the first-order dispersion of the grating. Both the output of the channeltron and the reference diode monitoring the incident laser energy were sent to a gated boxcar integrator and stored on a computer for further averaging and analysis.

The temporal characteristics of the x-ray emission were measured on single shots using a Kentech x-ray streak camera with 18-psec temporal resolution. The temporal resolution of the streak camera was calibrated using a 1-psec pulse of ultraviolet radiation at 290 nm. The time history of x-ray emission in an energy range of 50–70 eV was measured using a 0.75-μm-thick Al filter and a photocathode composed of 200 Å Al on 0.1 μm Formvar. X-ray emission in an energy range of 1.0–1.5 keV was measured using a filter of 0.5 μm Al on 0.3 μm parylene, with a photocathode of 1000 Å CsI on 3.8 μm Mylar.

Unless otherwise stated, the laser energy on target was 1 mJ and the polarization of the laser beam was in the plane of incidence (P polarized). The angle between the laser beam and the target normal was 25°, and the angle between the line of sight of the detector and the target normal was 60°.

RESULTS

The time-resolved x-ray emission measured from a Au target is shown in Fig. 2. Figures 2(a) and 2(b) are microdensitometer traces of single-shot streak records corresponding to the energy ranges of 50–70 eV and 1.0–1.5 keV, respectively. The x-ray pulse widths (FWHM) are 35 psec for the 50–70-eV band and 18 psec for the 1.0–1.5-keV band. Deconvolving the temporal response of the streak camera, we infer a pulse duration of 30 psec for the 50–70-eV band and an upper limit of 10 psec for the 1.0–1.5-keV band.

Time-integrated x-ray emission spectra for Si, Ti, and Au targets are presented in Fig. 3. All of the spectra are unfiltered except for the Au emission spectrum above 400 eV, which was filtered using a 0.5-μm Al–0.3-μm parylene foil. In all cases the spectra consist of lines or bands of emission broadened by the instrumental response, and superimposed on a background continuum. The x-ray yield, given in units of keV/keV into 2π steradians, has been absolutely calibrated with $\sim 50\%$ accuracy using an analysis of the photon statistics of the x-ray emission as discussed in the Appendix. The calibration is valid for either an isotropic or a Lambertian angular distribution of the emission.

Figure 4 shows the same Si, Ti, and Au spectra plotted per unit wavelength interval so that the emission lines are more easily visible. The transitions have been identified using computer calculations based on the relativistic Hartree-Fock average-configuration model.[7] The Si spectrum contains a $3d \rightarrow 2p$ and a $3s \rightarrow 2p$ band between 30–100 Å and a $2p \rightarrow 2s$ band between 200–300 Å. The lines are identified by the number of bound electrons remaining in the emitting ion. For Ti, the spectrum is dominated by a $3d \rightarrow 3p$ band between 230–320 Å while weaker $4s \rightarrow 3p$ and $4d \rightarrow 3p$ transitions are seen between

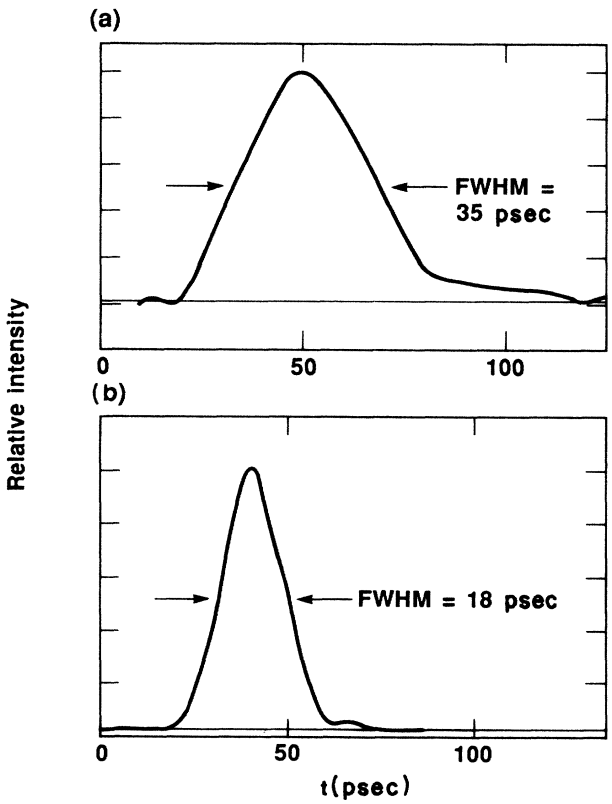

FIG. 2. Single-shot streak records of radiation emitted from a Au target, irradiated by a 1-mJ, 1-psec pulse preceded by a 3-nsec, 15-μJ prepulse. (a) 50–70-eV radiation. (b) 1.0–1.5-keV radiation. The time resolution of the streak camera was 18 psec.

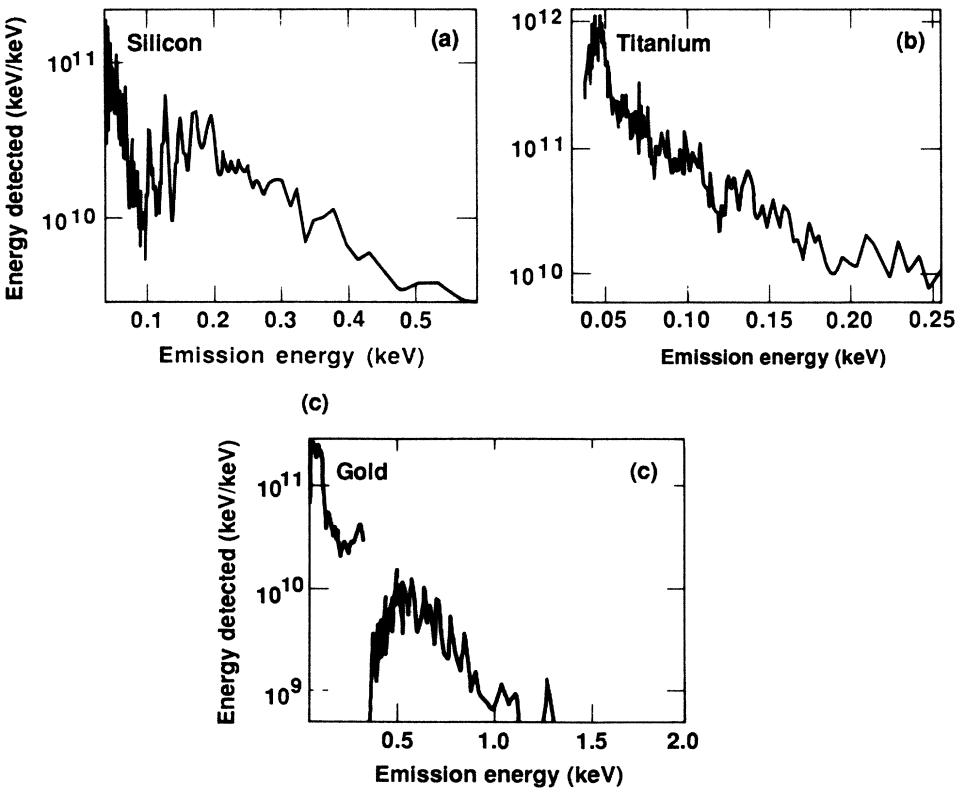

FIG. 3. Absolutely calibrated, time-integrated x-ray emission spectra: (a) Si, (b) Ti, (c) Au. The Au spectrum above 400 eV was filtered as described in the text, and has not been corrected for the filter response.

80–230 Å. The Au spectrum exhibits three distinct bands of emission at 30–40, 120–200, and 200–300 Å, corresponding to transitions into the $n=4$, 5, and 6 levels, respectively. These spectra indicate a considerable amount of ionization: at least 9, 10, and 19 electrons have been stripped off the Si, Ti, and Au atoms, respectively.

We observed that the x-ray yield varied significantly with both the energy and the angle of incidence of the laser beam, particularly at higher emission energies. The x-ray yield from a Au target in the 400–1000-eV band, measured as a function of incident laser energy, is shown in Fig. 5. The laser energy was varied using neutral density filters, so that the ratio of energies in the short and long pulses remained fixed. Each data point represents an average of 50–100 shots. The dependence of the x-ray yield Y on laser energy E is well described by a power law,

$$Y \propto E^{4.3} . \tag{1}$$

The x-ray yield in the 400–1000-eV band was measured as a function of the angle θ between the laser beam (P polarized) and the target normal, and is shown in Fig. 6(a). A strong peak in the yield is evident with the maximum occurring at $\sim 25°$. The x-ray yield for an S-polarized incident beam at 25° is shown for comparison, and exhibits a significantly reduced yield. Figure 6(b) shows a similar measurement of the angular dependence in the case where the nanosecond prepulse has been eliminated. The strong peak in emission at 25° is no longer observable and the overall x-ray yield is decreased by an order of magnitude.

DISCUSSION

The nature of the x-ray emission provides valuable information about the mechanisms responsible for the generation of ultrashort x-ray pulses. The dependence of the x-ray yield on the angle of incidence and the polarization of the laser beam is characteristic of resonance absorption.[8] In this absorption process, the component of the laser electric field along the plasma density gradient excites electron plasma waves at the critical density, where the local plasma frequency equals the laser frequency. The plasma waves convect to lower-density regions and some electrons are accelerated to high energies as the plasma waves are damped. These hot electrons thermalize rapidly and thus efficiently couple the laser energy into the plasma.

The absorption of the laser energy, and hence the x-ray emission, depends upon the strength of the electric field along the plasma density gradient at the critical density. For P-polarized light, the component of the electric field along the density gradient (i.e., normal to the target surface) increases with the angle of incidence. However, as the angle of incidence increases, the turning point of the laser beam occurs at lower density, so that the strength of the electric field that tunnels to the critical density is greatly reduced. It is the competition between these effects that causes the absorbed fraction of the laser ener-

gy $A(\theta)$ to have a strong maximum with an angular dependence given by[8]

$$A(\theta) \propto (kL)^{2/3} \sin^2\theta e^{-(4/3)kL\sin^3\theta} . \quad (2)$$

Here L is the electron density scale length at the critical density and k is the vacuum wave number of the laser radiation. The solid line in Fig. 6(a) represents the best fit of Eq. (2) to the data. To obtain this curve we have assumed that the x-ray yield consists of two components, a constant contribution arising from absorption mechanisms which are independent of the incident angle and the polarization of the laser beam and a contribution from resonance absorption proportional to $A^{4.3}$ [see Eq. (1)]. In addition, the curve has been broadened to correct for the 7° angular spread of the focused laser beam. Fitting Eq. (2) to the data yields an electron density scale length $L = 6000 \pm 1000$ Å. Since strong resonance absorption is not observed when the low-intensity long pulse is absent [Fig. 6(b)], we conclude that the 6000-Å scale-length plasma is produced by the heating of the solid target by the long pulse. Hence the existence of both laser pulses is required for the generation of an intense, ultrashort x-ray pulse. The long laser pulse preforms a plasma into which the energy of the short laser pulse is efficiently and rapidly coupled through resonance absorption. A similar mechanism is probably responsible for the enhanced x-ray yield recently reported from the irradiation of a solid target by two successive high-intensity (10^{17} W/cm^2), subpicosecond laser pulses.[9] A direct comparison of our results to this work is difficult, however, as the time scales and prepulse characteristics are very different.

The line and band emission seen in Fig. 4 clearly indicates that the harder x rays come from ionization states of up to $Z = +9$, $+10$ and $+19$ for Si, Ti, and Au, respectively. The long laser pulse, with an intensity of 10^9 W/cm^2, can only produce a 1–10-eV plasma.[10] Since the ratio of ionization potential χ to electron temperature T_e is typically 3–10 in plasmas not fully stripped, this corresponds to a maximum ion charge state of $Z \cong +3$ in Si, Ti, and Au. Hence the short laser pulse is responsible for generating ionization states between $Z = +4$ and $+19$, which is also consistent with the short duration of the x-ray emission.

We now consider in detail the mechanisms responsible for the generation of the ultrashort, high-energy (>1

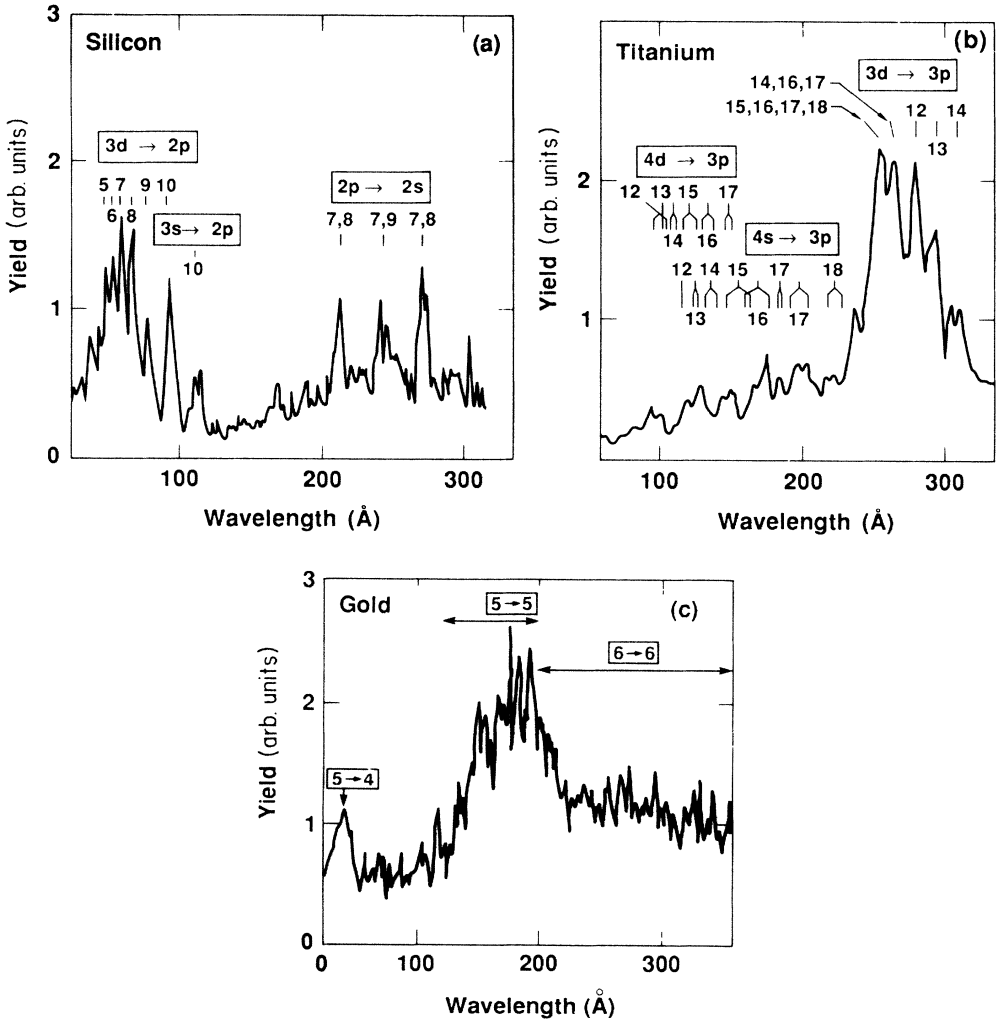

FIG. 4. Unfiltered time-integrated x-ray emission spectra exhibiting line and band emission: (a) Si, (b) Ti, (c) Au.

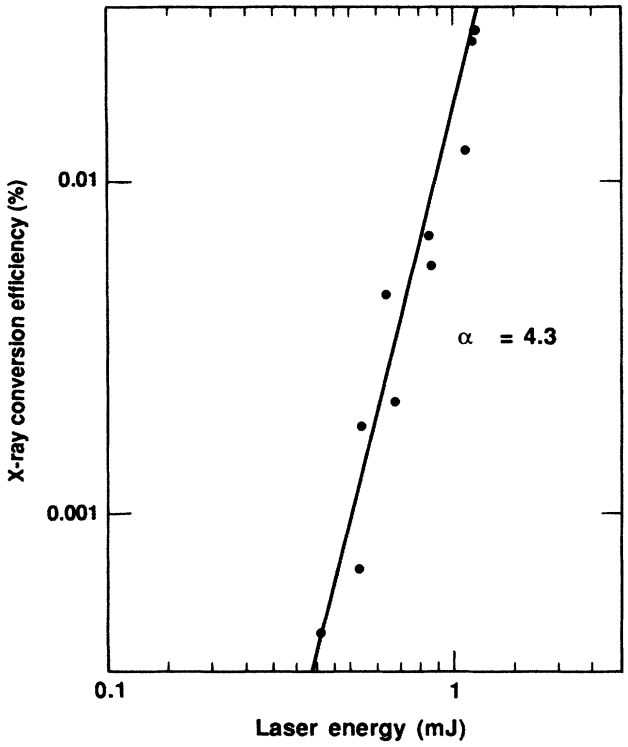

FIG. 5. Time-integrated x-ray conversion efficiency from a Au target in a 400–1000-eV band as a function of laser energy.

keV) x-ray emission observed from Au targets. The streak camera record [Fig. 2(b)] shows that the emission lasts for less than 10 psec. Hence a lower limit on the ionization rate up to $Z=+19$ can be set at 10^{11} sec^{-1}. We assume that hot electrons produced by resonance absorption thermalize through electron-electron collisions and rapidly increase the bulk plasma temperature near the critical density. The theoretical ionization rate S for a Maxwellian electron energy distribution is given by[11]

$$S=1.6\times10^{-6}N_e(T_e^{1/2}/\chi^2)e^{-\chi/T_e}\ , \tag{3}$$

where χ and T_e are in eV, N_e is in cm^{-3}, and S is in sec^{-1}. For an average ionization potential $\chi=250$ eV, and for $\chi/T_e=3$ and $\chi/T_e=10$ the ionization rates are, respectively, $S=10^{-11}N_e$ sec^{-1} and $S=10^{-14}N_e$ sec^{-1}. Hence the stripping of several electrons within 10 psec at the critical density ($N_e=3\times10^{21}$ cm^{-3}) is only feasible if $\chi/T_e<3$, implying that T_e is greater than 100 eV. We note that for $T_e=100$ eV and $N_e=3\times10^{21}$ cm^{-3}, the electron-electron thermalization time is 10 fsec,[12] much shorter than either the collisional ionization time or the laser pulse length, thus justifying the use of a Maxwellian electron energy distribution. Plasma temperatures in excess of 100 eV are consistent with earlier measurements[6] of x-ray emission from similar plasmas, where a temperature of $T_e=200\pm50$ eV was inferred from the measured blackbody radiation flux at 50 Å.

The duration of the x-ray emission, particularly at the higher energies, is determined by the rate at which the population of ions in the highly-charged states decreases. The ultrashort x-ray emission suggests that the decay of the population is rapid and that the ionization mechanisms that feed the population turn off within several picoseconds. The dominant decay mechanism is likely to be three-body collisional recombination. The recombination time τ for ions in charge state Z in a plasma with electron temperature T_e (in keV) and density N_e (in cm^{-3}) is given approximately by[13]

$$\tau=14T_e\left[\frac{10^{22}}{N_e}\right]\frac{1}{Z}\ \text{psec}\ . \tag{4}$$

For values of $N_e=3\times10^{21}$ cm^{-3}, $T_e=200$ eV, and $Z=19$ the recombination time is 0.5 psec. Hence the ion population will deplete rapidly provided that the ionization

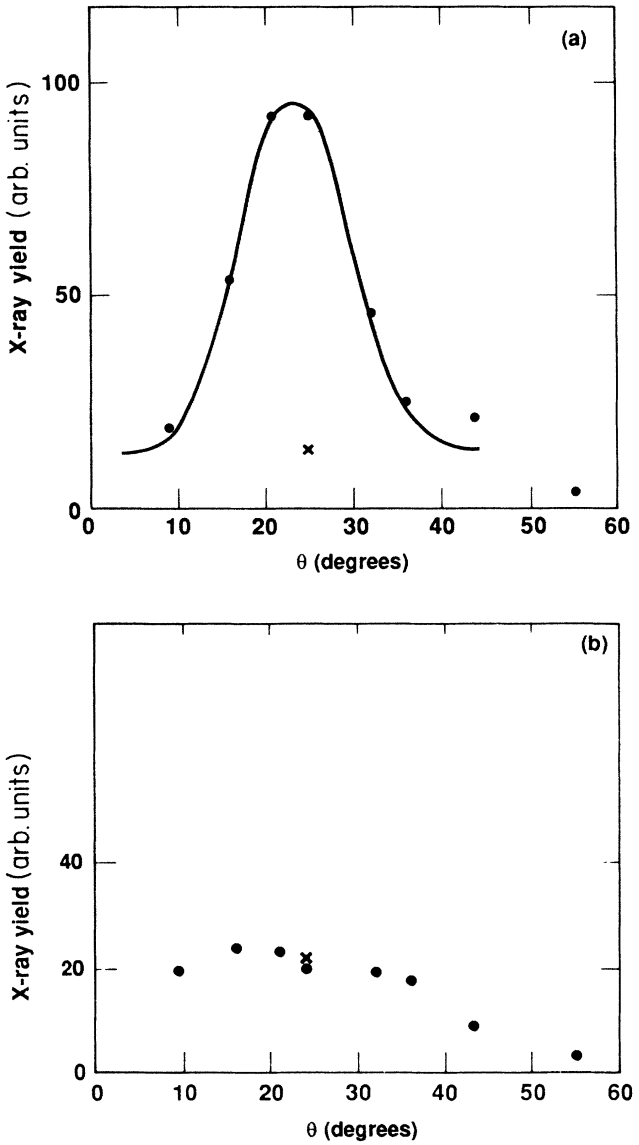

FIG. 6. Time-integrated x-ray yield from a Au target in a 400–1000-eV band as a function of the angle between the laser beam and target normal (●, P polarization; ×, S polarization). (a) High-intensity short pulse preceded by a low-intensity long pulse. The solid curve is a fit to Eq. (2). (b) Without the low-intensity long pulse.

processes cannot replenish the highly-charged states.

The ionization rate, given by Eq. (3), is strongly dependent on temperature. For an ionization potential of $\chi = 600$ eV, the ionization rate decreases by a factor of 20 when the electron temperature is decreased from 200 to 100 eV. We propose that the duration of the x-ray emission at the higher energies is limited by the time required for the plasma at the critical density to cool to a temperature at which the ionization rate is negligible. Rapid cooling will occur via thermal conduction into the cooler, overdense plasma. The cooling time can be estimated using the equation for heat conduction in a plasma,[14] assuming that the electron mean free path is shorter than the temperature scale length. The time t_c for a hot plasma slab of uniform density N_e, initial temperature T_e, and thickness x_0 to decrease in temperature by a factor of 2 is given by

$$t_c = \frac{2^{9/2}(2.6)N_e Z e^4 \sqrt{m_e} x_0^2 \ln\Lambda}{(4\pi\epsilon_0)^2 (kT_e)^{5/2}} \text{ SI units} . \quad (5)$$

Here Z is the average charge state in the cold plasma and $\ln\Lambda$ is the Coulomb logarithm. For $N_e = 3\times 10^{21}$ cm^{-3}, $T_e = 200$ eV, $Z = 3$, and x_0 taken to be the density scale length of 6000 Å, Eq. (5) yields a value of $t_c \sim 10$ psec. In a more rigorous investigation, the thermal conduction equation has been solved numerically for a variety of density profiles using the initial plasma temperatures of 200 eV below critical density and 10 eV above critical density, with a transition region of 6000 Å. The solutions show that the temperature at critical density reduces to 100 eV within 10 psec regardless of the exact form of the density profile, which is to be expected since the thermal conductivity has a very weak dependence on the electron density. Thus the ultrashort x-ray emission at higher energies is consistent with the rapid cooling of the plasma through thermal conduction.

CONCLUSION

Ultrashort x-ray pulses have been generated by the interaction of a high-intensity, picosecond laser pulse with a plasma produced by the irradiation of a solid target with a low-intensity laser pulse of several nanoseconds duration. In this scheme, energy in the short laser pulse is coupled efficiently into the electrons through resonance absorption in the preformed plasma, resulting in rapid increases in the electron temperature and ionization state. After the short laser pulse is off, the hot plasma at critical density cools rapidly through thermal conduction into the overdense region.

The x-ray emission spectra typically exhibit a series of identifiable lines superimposed on a broadband continuum. The duration of the x-ray emission decreases with increasing energy, becoming <10 psec in the 1-keV range. We have measured an x-ray yield from Au targets of 10^9 keV/keV at an emission energy of 1 keV. The equivalent brightness of the x-ray pulse (a standard measure of the strength of an x-ray source) is 10^{20} photons/sec mm^2 eV into 2π steradians. This is orders of magnitude brighter than most other sources, being comparable to synchrotron radiation enhanced by insertion devices such as undulators. It is, in fact, probable that the x-ray yield in the present experiment was not optimized, owing to the fixed configuration of the prepulse. Experiments are in progress to study the x-ray emission as a function of the relative intensity and delay between the prepulse and the high-intensity short pulse.

The ultrashort, intense x-ray pulse described in this paper represents a source with many useful features for application in high-resolution time-resolved measurements. The intrinsic synchronization of the x-ray pulse with the short optical pulse is ideally suited to pulse-probe techniques, and allows for low-jitter triggering of electronics such as gated detectors. The present maximum repetition rate of 10 Hz permits a moderate amount of signal averaging. Furthermore, the x-ray source is broadband in the sense that a wide range of energies can be accessed by the proper choice of target material. Specific applications for such a source include time-resolved x-ray diffraction and EXAFS in order to study dynamical changes in, respectively, the long-range and short-range order of condensed matter. Another important application is flash radiography, in which a dynamic system can be backlit by the ultrashort x-ray pulse to obtain an image of the instantaneous absorption profile. For the laser power levels used in this work, the x-ray emission is restricted to energies less than ~ 1 keV. It is likely, however, that by using a higher power, short-pulse laser ions can be stripped to core levels, producing ultrashort x-ray pulses with significant brightness in the energy range of 1–10 keV.

ACKNOWLEDGMENTS

We gratefully acknowledge the assistance of B. M. Cook, M. Perry, and R. L. Hanks in the design and assembly of the experimental apparatus. This work was performed under the auspices of the U.S. Department of Energy by the Lawrence Livermore National Laboratory under Contract No. W-7405-ENG-48.

APPENDIX

In this appendix we show how the photon statistics associated with the x-ray emission can be used to absolutely calibrate the x-ray yield. Consider the average x-ray signal $\bar{S}$ measured from N shots detected by the channeltron. Then,

$$\bar{S} = m\eta\bar{G} , \quad (A1)$$

where m is the average number of x rays incident on the channeltron detector, η is the quantum efficiency of the channeltron, and $\bar{G}$ is the average gain of the channeltron. The variance of the signal σ_S^2 is the sum of three factors associated with the variances of each stage in the detection process. The first stage consists of the number of photons m incident on the channeltron. The standard deviation in the number of photons is $m^{1/2}$. This is subsequently amplified to yield a variance in the signal of

$$\sigma_1^2 = (m^{1/2}\eta\bar{G})^2 = m\eta^2\bar{G}^2 . \quad (A2)$$

The second stage corresponds to the interaction of an x

ray with the photocathode of the channeltron. The probability of the x ray generating a photoelectron is η, and the probability of not generating a photoelectron is $1-\eta$. For m incident x rays the problem is equivalent to a biased random walk with m steps, so that the standard deviation in the number of detected x rays is $[m\eta(1-\eta)]^{1/2}$. This is subsequently amplified to yield a variance of

$$\sigma_2^2=\{[m\eta(1-\eta)]^{1/2}\bar{G}\}^2=m\eta(1-\eta)\bar{G}^2 . \quad \text{(A3)}$$

The third stage corresponds to the gain of the channeltron, which has a variance σ_G^2. We consider each detected x ray to be an independent event so that the total variance of this stage is

$$\sigma_3^2=m\eta\sigma_G^2 . \quad \text{(A4)}$$

The variance in the signal is given by

$$\begin{aligned}\sigma_S^2&=\sigma_1^2+\sigma_2^2+\sigma_3^2\\&=m\eta^2\bar{G}^2+m\eta(1-\eta)\bar{G}^2+m\eta\sigma_G^2\\&=\bar{G}\,\bar{S}(1+\sigma_G^2/\bar{G}^2) .\end{aligned} \quad \text{(A5)}$$

When the channeltron detector is operated in the analog output mode, the distribution function $W(G)$ that represents the variation in the gain can be modeled as an exponential:[15]

$$W(G)=\frac{1}{\bar{G}}e^{-G/\bar{G}} . \quad \text{(A6)}$$

This distribution has a variance $\sigma_G^2=\bar{G}^2$. Hence,

$$\sigma_S^2=2\bar{G}\,\bar{S} . \quad \text{(A7)}$$

The quantities $\bar{S}$ and σ_S^2 are experimentally determined by measuring the signal S_i on N shots and applying the well-known formulas:

$$\bar{S}=\frac{1}{N}\sum_i S_i , \quad \text{(A8)}$$

$$\sigma_S^2=\frac{1}{N-1}\sum_i (S_i-\bar{S})^2 . \quad \text{(A9)}$$

It is important to select a set of measurements S_i that correspond to the same incident laser energy, in order to eliminate variations in the signal due to laser energy fluctuations. Equation (A7) can then be used to determine the gain $\bar{G}$ of the channeltron. The quantum efficiency of the channeltron as a function of x-ray energy is available in the literature.[15] Then the absolute number of photons incident on the channeltron is given by $m=\bar{S}/(\eta\bar{G})$. To determine the absolute yield of x rays at a particular energy it is necessary to also know the efficiency of the transmission grating. The efficiency of the grating has been independently measured and was found to be 0.06 into zeroth order and 0.01 into first order. The efficiency is relatively constant for energies less than 1 keV.

[1]*Picosecond Phenomena III*, edited by K. B. Eisenthal, R. M. Hochstrasser, W. Kaiser, and A. Laubereau (Springer-Verlag, Berlin, 1982).
[2]B. C. Larson, C. W. White, T. S. Noggle, and D. Mills, Phys. Rev. Lett. **48**, 337 (1982).
[3]P. J. Mallozzi, R. E. Schwerzel, H. M. Epstein, and B. E. Campbell, Science **206(10)**, 355 (1979).
[4]R. W. Eason, D. K. Bradley, P. J. Dobson, and J. D. Hares, Appl. Phys. Lett. **47**, 442 (1985).
[5]N. M. Ceglio, R. L. Kauffman, A. M. Hawryluk, and H. Medecki, Appl. Opt. **22**, 318 (1983).
[6]O. L. Landen, E. M. Campbell, and M. D. Perry, Opt. Commun. **63**, 253 (1987).
[7]C. L. Cocke, S. l. Varghese, J. A. Bednar, C. P. Bhalla, B. Curnutte, R. Kauffman, R. Randall, P. Richard, C. Woods, and J. H. Scofield, Phys. Rev. A **12**, 2413 (1975).
[8]V. L. Ginzburg, *The Propagation of Electromagnetic Waves in Plasmas* (Pergamon, New York, 1970), p. 260.
[9]D. Kühlke, U. Herpers, and D. von der Linde, Appl. Phys. Lett. **50**, 1785 (1987).
[10]G. Wallis, Contrib. Plasma Phys. **22**, 295 (1982).
[11]M. Gryzinski, Phys. Rev. **138**, 336 (1965).
[12]L. Spitzer, Jr. and R. Härm, Phys. Rev. **89**, 977 (1952).
[13]D. W. Phillion and C. J. Hailey, Phys. Rev. A **34**, 4886 (1986).
[14]Y. B. Zel'dovich and Y. P. Raizer, *Physics of Shock Waves and High-Temperature Hydrodynamic Phenomena* (Academic, New York, 1967), p. 663.
[15]J. L. Wiza, Nucl. Instrum. Methods **162**, 587 (1979).